Pergamon

Int. J. Heat Mass Transfer. Vol. 39, No. 10, pp. 2165–2175, 1996

0017-9310/96 $15.00+0.00

0017-9310(95)00208-1

Thermal enhancement in laminar channel flow with a porous block

WU-SHUNG FU, HSIN-CHIEN HUANG and WEI-YAN LIOU

Department of Mechanical Engineering, National Chiao Tung University, Hsinchu, 30050, Taiwan, Republic of China

(*Received* 10 *January* 1995 *and in final form* 20 *June* 1995)

Abstract—A study of a porous block mounted on a heated wall in a laminar flow channel to enhance convection heat transfer rate was investigated numerically. A numerical method of SIMPLEC is adopted to solve governing equations, as for the energy equation, one-equation thermal model with Van Driest's wall function is considered. The parameters that include porosity ε, particle diameter D_p, Reynolds number Re, and blocked ratio HP are studied, and for simulating more realistically, the porosity is taken into consideration as variable. All the non-Darcian effects including the channeling effects, solid boundary effects, and inertial effects are also considered. The effects of the above parameters on the thermal performance of the heated wall are examined in detail. The results indicate that for $HP = 0.5$ case the thermal performances are enhanced by using a porous block with higher porosity and particle diameter. However, the results are the opposite for $HP = 1.0$. Copyright © 1996 Elsevier Science Ltd.

INTRODUCTION

Porous media have large contact surfaces with fluids which enhance heat transfer performance, hence, there are wide investigations of heat transfer and transport phenomena in the porous media for many industrial applications such as heat exchangers, the packed-sphere bed, electronic cooling, chemical catalytic reactors, drying processes, heat pipe technology, etc.

Vafai and Tien [1] used volume-averaging technique to derive the transport equations describing the effects of both the solid boundary and inertia forces on flow and heat transfer in porous media. The non-Darcian effects, including the solid boundary and inertia effects, were more noticeable for high porosity, high Prandtl number and large pressure gradients. Kaviany [2] investigated heat transfer in porous media bounded by two isothermal parallel plates in laminar forced convection. The results showed that the Nusselt number in the fully developed region increased with increasing porous media shape factor γ $(= (H^2\varepsilon/K)^{1/2})$. Benenati and Brosilow [3] measured the porosity variation in packed beds and showed that the porosity was a function of the distance from the boundary. Vafai [4] analyzed the influences of channeling effect and inertia forces on convection flow and heat transfer in porous media, and found that the channeling effect indicated a significant influence on the increase of the Nusselt number for high porosity and high Reynolds number conditions. Vafai *et al.* [5] used both experimental and numerical methods to study forced convective heat transfer in uniform-size-bead porous media. The aspect ratio of the above test section was equal to 4, and the non-Darcian effects included solid boundary effect, inertia effect and channeling effect. The results mentioned that the deviation between experimental and numerical analyses may be induced by both the channeling effect and solid boundary effect being neglected in the numerical computation. Hence all non-Darcian effects which included channeling effect, inertial effect, and solid boundary effect should be considered for obtaining more reliable results of transport phenomena in porous media.

The energy equations of fluid and porous material in most previous studies were combined into one equation, i.e. one-equation model, with the assumption of local thermal equilibrium. Cheng and Hsu [6] used the two-layer mixing length theory to study the effects of transverse thermal dispersion in the near wall region of porous media. Afterward, Cheng and his co-workers [7–10] used Van Driest's mixing length theory (wall function) instead of two-layer mixing length to solve the same problems. As a result, the utilization of the Van Driest's wall function was more convenient than that of the two-layer mixing length theory for solving complex heat transfer problems in porous media.

Recently, much research has been focused on the interfacial problem of the fluid–porous media composite system. The conditions of the velocity and temperature on the interface between the two different materials are complicated. Beavers and Joseph [11] presented an empirical correlation for the velocity gradient at the interface in terms of the velocities in the external flow and the porous media. Vafai and Thiyagaraja [12] considered three general cases of the above problems which included the interface between two different porous media, the interface between

NOMENCLATURE

- B_o coefficient in the stagnant conductivity
- C_f specific heat of fluid [kJ kg^{-1} °C^{-1}]
- d_P particle diameter [m]
- Da Darcy number
- D_P ratio of particle diameter to the length of the porous block, $D_P = d_P/L_P$
- D_1 empirical constant in thermal dispersion conductivity
- F inertial factor
- h_x heat transfer coefficient along the X direction [W m^{-2} °C^{-1}]
- H height of the channel [m]
- H_P height of the porous block [m]
- HP blocked ratio, $HP = H_P/H$
- k_d stagnant conductivity [W m^{-1} °C^{-1}]
- k_e effective thermal conductivity of the porous block [W m^{-1} °C^{-1}]
- k_f thermal conductivity of the fluid [W m^{-1} °C^{-1}]
- k_s thermal conductivity of solid phase in porous block [W m^{-1} °C^{-1}]
- k_t thermal dispersion conductivity [W m^{-1} °C^{-1}]
- K permeability [m^2]
- l Van Driest's wall function
- L_1 length of the channel [m]
- L_2 distance from the inlet to the front side of the porous block [m]
- L_3 downstream distance from the porous block to the exit [m]
- L_P length of the porous block [m]
- $\dot{m}$ mass flow rate [kg s^{-1}]
- $\vec{n}$ outward normal vector on the interfacial surface [m^{-1}]
- Nu_x local Nusselt number along the X direction
- Nu_s local Nusselt number along the interfacial surface of the porous block
- p dimensional pressure [N m^{-2}]
- P dimensionless pressure
- Pr Prandtl number
- r_1, r_2 coefficient in equation (1)
- Re Reynolds number, $Re = u_o H/\nu_f$
- Re_P particle diameter based Reynolds number, $Re_P = u_P^* d_P/\nu_f$
- Δs shortest distances from the calculated point to the boundaries of the porous block [m]
- S dimensionless distance along the interfacial surface from the bottom left corner of the porous block
- T temperature [°C]
- u dimensional velocity in the x direction [m s^{-1}]
- u_o mean inlet velocity [m s^{-1}]
- u_P^* mean velocity inside the porous block in the x direction [m s^{-1}]
- U dimensionless velocity in the X direction
- v dimensional velocity in the y direction [m s^{-1}]
- V dimensionless velocity in the Y direction
- x, y dimensional Cartesian coordinate [m]
- X, Y dimensionless Cartesian coordinate.

Greek symbols

- $\Delta X_{min}, \Delta Y_{min}$ dimensionless minimum mesh size in X and Y direction
- Ψ dimensionless stream function
- Φ computational variable
- Λ ratio of thermal conductivity of solid phase to fluid phase in porous block
- α thermal diffusivity [m^2 s^{-1}]
- ε porosity [m^3 m^{-3}]
- ε_e effective porosity [m^3 m^{-3}]
- γ shape factor, $\gamma = (H^2\varepsilon/K)^{1/2}$
- μ viscosity [kg m^{-1} s^{-1}]
- ν kinematic viscosity [m^2 s^{-1}]
- θ dimensionless temperature
- ρ fluid density [kg m^{-3}]
- ω empirical constant in Van Driest's wall function
- $|\ |$ magnitude of velocity vector.

Superscript

- n the nth iteration index
- $\bar{}$ mean value
- $\rightarrow$ velocity vector.

Subscript

- C.V. control volume
- e effective value
- f external flow field
- p porous media
- o inlet condition
- w solid wall of the porous block
- wpb without-porous-block case.

porous media and an external fluid field, and the interface between porous media and a solid boundary. Both the numerical method and theoretical derivation were adopted. The numerical results were found to be good in agreement with analytical results. Vafai and Kim [13] derived an exact solution for the same problem studied by Beavers and Joseph [11] and both the effects of Darcy number and inertia parameter were investigated. Vafai and Kim [14] also studied the thermal performance for a composite porous–fluid system. The porosity and the effective thermal conductivity were assumed constant. The enhancement of thermal performance of the porous media mainly depended on the ratio of the effective thermal conductivity of the porous media to fluid thermal conductivity. As the ratio was very large, the enhancement of thermal performance is obtained, otherwise, the heat transfer rate decreased. Huang and Vafai [15] studied the heat transfer of a flat plate mounted with porous block array. The porosity ε was regarded as constant, the channeling effect in the near wall region and the thermal dispersion were both neglected. The porous block array significantly reduced the heat transfer rate on the flat plate shown in the results. However, different trends were obtained by Hadim [16]. He investigated two configurations of a fully porous channel and a partially divided porous channel. The results indicated that the partially divided porous channel configuration was an attractive heat transfer augmentation technique, although the ratio of the effective thermal conductivity of the porous media to fluid thermal conductivity was equal to 1. Huang and Vafai [17] indicated four effects of penetrating, blowing, suction and boundary layer separation on the flow and thermal fields in a channel mounted with porous arrays. In the above literature, the porosity of the porous media was usually regarded as a constant. However, due to the influence of the impermeable wall, the porosity of the porous media near the solid boundary is hardly constant [4].

The aim of this numerical study intends to adopt a porous block mounted on a heated plate in a horizontal channel to enhance thermal performance in laminar flow. For simulating the model more realistically, the factor of variable porosity is considered. The other factors of the particle diameter D_P, blocked ratio HP, Reynolds number of external flow field Re, and the non-Darcian effects including the channeling effect, solid boundary effect and inertial effect are also taken into consideration. As for the thermal dispersion, the one-equation model is adopted at present. The results indicate that the thermal performances are enhanced by using the porous block with higher porosity and particle diameter for the $HP = 0.5$ cases. However, the results are the opposite for $HP = 1.0$ cases.

PHYSICAL MODEL

The physical model in this study is shown in Fig. 1. There is a two-dimensional horizontal channel with height H and length L_1, respectively. The entrance length is L_2, the length and temperature of the high temperature region are L_p, which is equal to $H/2$, and T_w, respectively. A porous block with height H_p is mounted on the high temperature region and the other places of the channel are insulated. The porous block is composed of spherical beads. The length from the porous block to the exit is L_3 which is long enough for the fully developed distributions of the velocity and temperature to be formed. The inlet velocity profile is a fully developed parabolic type with average value u_o, and the inlet temperature is T_o which is smaller than T_w. Under this configuration, the flow field can be decomposed into two conjugate regions, one stands for the internal flow field where is bounded by the porous block, and the other is called the external flow field which excludes the porous media.

In order to simplify the problem, there are some assumptions as follows:

(1) The porous block is made of spherical beads. It is non-deformable and does not have any chemical reaction with the fluids.

(2) The flow field is steady-state, two-dimensional, single phase, laminar and incompressible.

(3) The fluid properties are constant and the effect of the gravity is neglected.

(4) The transverse thermal dispersion is modeled by Van Driest's wall function [7], hence one-equation model of energy equation is used.

(5) The effective viscosity of the porous media is equal to the viscosity of the external fluid.

The porosity ε, permeability K, and inertia factor F are defined as [4]

$$\varepsilon = \varepsilon_e[1+r_1\,e^{-r_2\Delta s/d_p}] \tag{1}$$

$$K = \frac{\varepsilon^3 d_p^2}{150(1-\varepsilon)^2} \tag{2}$$

$$F = \frac{1.75}{\sqrt{(150)}\varepsilon^{1.5}} \tag{3}$$

where the Δs is the shortest distance from the cal-

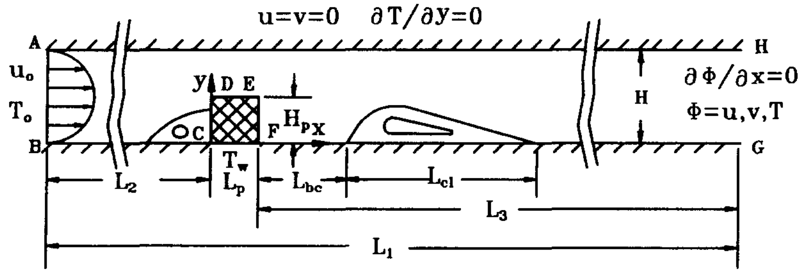

Fig. 1. Physical model.

culated point to the boundaries of the porous block, and r_1 and r_2 are both empirical constants.

The effective thermal conductivity of porous media k_e is a combination of stagnant conductivity k_d and thermal dispersion conductivity k_t [7] to simulate the transverse thermal dispersion. Then the relationship between k_e, k_d and k_t is

$$k_e = k_d + k_t \quad (4)$$

and k_d is defined as

$$\frac{k_d}{k_f} = 1 - \sqrt{(1-\varepsilon)} + \frac{2\Lambda\sqrt{(1-\varepsilon)}}{\Lambda - B_o} \times \left[\frac{B_o\Lambda(\Lambda-1)}{(\Lambda-B_o)^2}\ln\left(\frac{\Lambda}{B_o}\right) - \frac{B_o+1}{2} - \frac{\Lambda(B_o-1)}{\Lambda-B_o}\right] \quad (5)$$

where

$$\Lambda = \frac{k_s}{k_f} \quad (6)$$

$$B_o = 1.25\left(\frac{1-\varepsilon}{\varepsilon}\right)^{10/9} \quad (7)$$

and the k_t is defined by Van Driest's wall function as

$$\frac{k_t}{k_f} = D_T Pr Re_p |\vec{u}_p| l \quad (8)$$

where D_T is an empirical constant, and Re_p is partical diameter based Reynolds number, defined as

$$Re_p = \frac{u_p^* d_p}{\nu_f} \quad (9)$$

where the u_p^* is the mean velocity inside the porous media in the x direction and defined as

$$u_p^* = \frac{1}{H^p}\int_0^{H_p} u_p|_{x=0}\,dy \quad (10)$$

and l is the Van Driest's wall function and defined as

$$l = 1 - e^{-As/\omega d_p} \quad (11)$$

where the ω is an empirical constant.

Based on the above assumptions and with the following characteristic scales of H, $T_w - T_o$, ρu_o^2 and u_o, the governing equations, boundary conditions and interfacial conditions are normalized as follows:

(1) Governing equations of the external flow field

continuity equation

$$\frac{\partial U_f}{\partial X} + \frac{\partial V_f}{\partial Y} = 0 \quad (12)$$

X-momentum equation

$$U_f\frac{\partial U_f}{\partial X} + V_f\frac{\partial U_f}{\partial Y} = -\frac{\partial P_f}{\partial X} + \frac{1}{Re}\left(\frac{\partial^2 U_f}{\partial X^2} + \frac{\partial^2 U_f}{\partial Y^2}\right) \quad (13)$$

Y-momentum equation

$$U_f\frac{\partial V_f}{\partial X} + V_f\frac{\partial V_f}{\partial Y} = -\frac{\partial P_f}{\partial Y} + \frac{1}{Re}\left(\frac{\partial^2 V_f}{\partial X^2} + \frac{\partial^2 V_f}{\partial Y^2}\right) \quad (14)$$

energy equation

$$U_f\frac{\partial \theta_f}{\partial X} + V_f\frac{\partial \theta_f}{\partial Y} = \frac{1}{RePr_f}\left(\frac{\partial^2 \theta_f}{\partial X^2} + \frac{\partial^2 \theta_f}{\partial Y^2}\right). \quad (15)$$

(2) Governing equations of the internal flow field [10]

continuity equation

$$\frac{\partial U_p}{\partial X} + \frac{\partial V_p}{\partial Y} = 0 \quad (16)$$

X-momentum equation

$$U_p\frac{\partial}{\partial X}\left(\frac{U_p}{\varepsilon}\right) + V_p\frac{\partial}{\partial Y}\left(\frac{U_p}{\varepsilon}\right) = -\frac{\partial P_p}{\partial X} + \frac{1}{Re}\left(\frac{\partial^2 U_p}{\partial X^2} + \frac{\partial^2 U_p}{\partial Y^2}\right) - \frac{1}{ReDa}\varepsilon U_p - \frac{F|\vec{U}_p|}{\sqrt{Da}}\varepsilon U_p \quad (17)$$

Y-momentum equation

$$U_p\frac{\partial}{\partial X}\left(\frac{V_p}{\varepsilon}\right) + V_p\frac{\partial}{\partial Y}\left(\frac{V_p}{\varepsilon}\right) = -\frac{\partial P_p}{\partial X} + \frac{1}{Re}\left(\frac{\partial^2 V_p}{\partial X^2} + \frac{\partial^2 V_p}{\partial Y^2}\right) - \frac{1}{ReDa}\varepsilon V_p - \frac{F|\vec{U}_p|}{\sqrt{Da}}\varepsilon V_p \quad (18)$$

energy equation

$$U_p\frac{\partial \theta_p}{\partial X} + V_p\frac{\partial \theta_p}{\partial Y} = \frac{\partial}{\partial X}\left(\frac{1}{RePr_p}\frac{\partial \theta_p}{\partial X}\right) + \frac{\partial}{\partial Y}\left(\frac{1}{RePr_p}\frac{\partial \theta_p}{\partial Y}\right) \quad (19)$$

where

$$X = x/H \quad Y = y/H$$

$$U_f = u_f/u_o \quad V_f = v_f/u_o \quad P_f = p_f/\rho u_o^2$$

$$U_p = u_p/u_o \quad V_p = v_p/u_o \quad P_p = p_p/\rho u_o^2$$

$$\theta_f = (T_f - T_o)/(T_w - T_o) \quad \theta_p = (T_p - T_o)/(T_w - T_o)$$

$$Pr_f = \nu_f/\alpha_f \quad Pr_p = \nu_p/\alpha_p$$

$$\alpha_f = k_f/\rho_f C_f \quad \alpha_p = k_e/\rho_f C_f \quad Da = K/H^2$$

$$Re = u_o H/\nu_f \quad |\vec{U}_p| = \sqrt{(U_p^2 + V_p^2)}. \quad (20)$$

(3) Boundary conditions

on surface AH, BC and FG

$$U_f = 0 \quad V_f = 0 \quad \frac{\partial \theta_f}{\partial Y} = 0 \quad (21)$$

on surface AB

$$U_f = -6(Y^2 - Y) \quad V_f = 0 \quad \theta_f = 0 \tag{22}$$

on surface HG

$$\frac{\partial U_f}{\partial X} = 0 \quad \frac{\partial V_f}{\partial X} = 0 \quad \frac{\partial \theta_f}{\partial X} = 0 \tag{23}$$

on surface CF

$$U_p = 0 \quad V_p = 0 \quad \theta_p = 1. \tag{24}$$

(4) Interfacial conditions, based on [13–17]

on surface CD and EF

$$U_f = U_p \quad V_f = V_p \quad P_p = P_f$$

$$\frac{\partial U_f}{\partial X} = \frac{\partial U_p}{\partial X} \quad \frac{\partial V_f}{\partial X} = \frac{\partial V_p}{\partial X}$$

$$\theta_f = \theta_p \quad k_f \frac{\partial \theta_f}{\partial X} = k_e \frac{\partial \theta_p}{\partial X} \tag{25}$$

on surface DE

$$U_f = U_p \quad V_f = V_p \quad P_p = P_f$$

$$\frac{\partial U_f}{\partial Y} = \frac{\partial U_p}{\partial Y} \quad \frac{\partial V_f}{\partial Y} = \frac{\partial V_p}{\partial Y}$$

$$\theta_f = \theta_p \quad k_f \frac{\partial \theta_f}{\partial Y} = k_e \frac{\partial \theta_p}{\partial Y}. \tag{26}$$

NUMERICAL METHOD

The SIMPLEC algorithm [18] with TDMA solver [19] is used to solve the governing equations (12)–(19) of the flow and the thermal fields. The equations (12)–(19) are first discretized into algebraic equations by using control volume method [19] with power-law scheme. Underlaxation factors are 0.5 for both the fields of velocity and temperature. The conservation residues [18] of the equations of momentum, energy and continuity and the relative errors of each variable are used to examine the convergence criteria which are defined as follows:

$$\left(\sum |\text{Residue of } \Phi \text{ equation}|^2_{\text{c.v.}}\right)^{1/2} \leqslant 10^{-4},$$

$$\Phi = U, V, \theta \quad \text{and mass flow rate} \tag{27}$$

$$\frac{\max|\Phi^{n+1} - \Phi^n|}{\max|\Phi^{n+1}|} \leqslant 10^{-5} \quad \Phi = U, V, P, \theta. \tag{28}$$

For reducing computation time, the non-staggered mesh is used. The finer meshes are set on both the interfacial regions of the porous block and near the solid wall regions. Then the meshes are expanded outward from the interfacial boundary and the solid wall with a scale ratio 1.2. In order to consider the channeling effect and the transverse thermal dispersion, the minimum mesh near the solid wall region and interfacial region should be less than two particle diameters, i.e. $\Delta X_{\min} \leqslant 2d_p/H$. Under the same reason, $\Delta Y_{\min}$ should be also less than $2d_p/H$.

On the basis of the suggestions of Patankar [19], the harmonic mean formulation of thermophysical properties is used to avoid the effects of abrupt change of these properties across the interfacial region of the porous block and the external flow field on the computation accuracy.

In Fig. 2(a), the results of this study are compared with those of Hadim [16]. The porosity ε_e and Darcy number are constant. The deviation between these two results is small. Figure 2(b) shows the comparisons between the results of Vafai [4] and this study, the deviation of maximum velocity is about 0.85%. Shown in Fig. 2(c), the results of Cheng and Hsu [7] under the one-equation thermal model of the porous media with the Van Driest's wall function situation are compared with those of this study for the case of $Re_p = 321$. The maximum deviation is about 0.72%.

The main parameters which include Reynolds number Re, blocked ratio HP, particle size ratio D_p, and effective porosity ε_e adopted in this study are tabulated in Table 1. The Darcy number Da listed in Table 1 is based on the effective porosity ε_e. Since the porosity ε is a variable as shown in equation (1), hence the Da in each control volume is also a variable during the computations. For the $Re = 500$ cases the entrance length L_2 is $7.5H$ and the downstream length L_3 from the rear side of block to the outlet is $50H$, and the fully developed conditions at the outlet section can be satisfied. For the cases of $Re = 1000$, the entrance and downstream lengths of the channel are $5H$ and $100H$, respectively.

Table 2 shows the empirical constants used in the definitions of the porosity ε [equation (1)] and the Van Driest's wall function l [equation (11)]. Where r_1 and r_2 of the $\varepsilon_e = 0.5$ cases are obtained from Vafai [4], but those of the $\varepsilon_e = 0.7$ cases are determined by the condition of the porosity near the wall approaching to unity. The D_T and ω are provided by Cheng and Hsu [7].

Due to the grid tests, the meshes of 132×60 and 144×60 are chosen for the cases of $Re = 500$ and 1000, respectively.

RESULTS AND DISCUSSION

The material of the spherical bead adopted in this study is considered as copper for enhancing the thermal performance.

Shown in Fig. 3, there are streamlines and isotherms for $Re = 500$, $HP = 0.5$, $D_P = 0.1$ and $\varepsilon_e = 0.5$ and 0.7 cases. The dimensionless stream function Ψ is defined as:

$$U = \frac{\partial \Psi}{\partial Y} \quad \text{and} \quad V = -\frac{\partial \Psi}{\partial X}. \tag{29}$$

For illustrating the flow and thermal fields more clearly, the phenomena in the region of $2HP$ upstream and $10HP$ downstream from the porous block are presented only. In Fig. 3(a), two recirculation zones are found in both the upstream and downstream

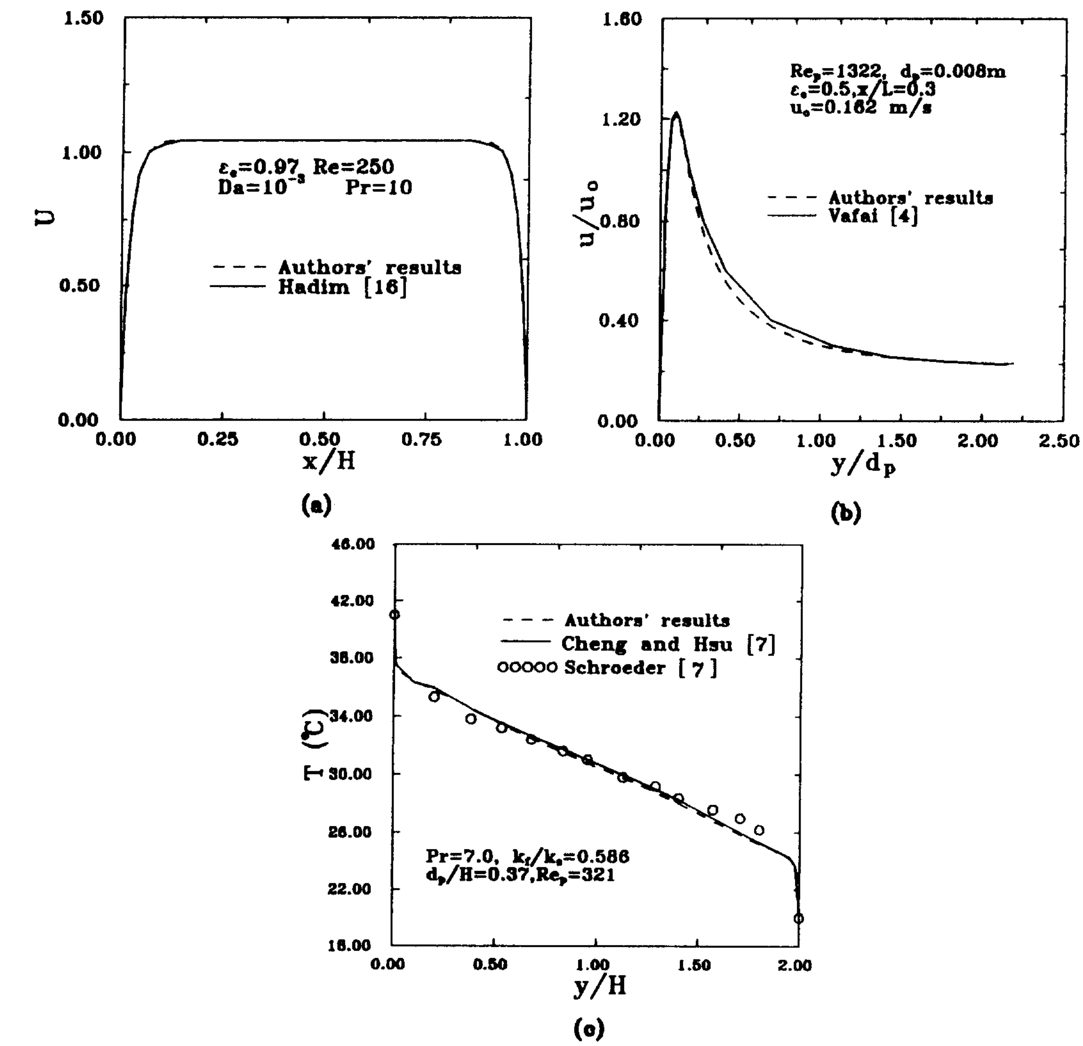

Fig. 2. The results compared with other literature: (a) U velocity profiles compared with Hadim [16]; (b) U velocity profiles with channeling effect compared with Vafai [4] and (c) temperature distribution with variable porosity compared with Cheng *et al.* [7].

Table 1. The main parameters

Re	HP	D_p	ε_c	Da	Pr
500	0.5	0.05	0.5	2.08E-6	
1000	1.0	0.1	0.7	|	0.7
		0.2		2.54E-4	

Table 2. The empirical constants

ε_c	r_1	r_2	D_T	ω
0.5	0.98	2	0.3	3.5
0.7	0.42			

regions of the porous block. Some fluid penetrated into the porous block which resulted in the downstream recirculation zone hardly neighboring the porous block. Near the solid wall the porosity is larger, then the fluid flows along and close to the solid wall. A small recirculation zone exists upstream which causes the isotherms [Fig. 3(b)] to extend upstream. As ε_c becomes larger ($= 0.7$), the fluid flows through the porous block more easily. Consequently, as shown in Fig. 3(c), the recirculation zone formed downstream is further away from the porous block, and the recirculation zone is barely observed in the upstream region. Meanwhile, the isotherms indicated in Fig. 3(d) extend downstream more conspicuously.

As shown in Fig. 4, the variations of the velocity distribution of U at the middle ($X = 0.25$) of the porous block are illustrated. Due to the channeling effect, the velocity of U has the maximum value near the solid wall. The larger the porosity is, the higher the velocity becomes. Near the wall, the velocity gradients of both porous cases are larger than that of the case without the porous block.

The normal velocity vector distributions along the interfacial surfaces of the porous block are shown in

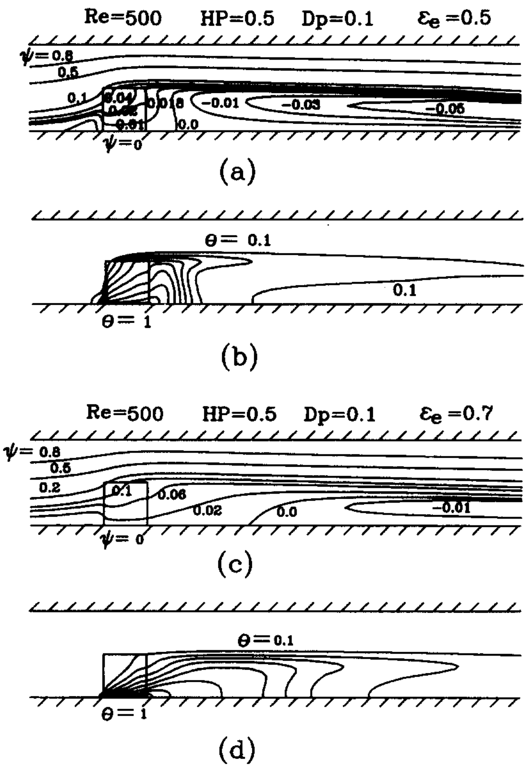

Fig. 3. Effects of variable porosity on flow field and thermal field ($Re = 500$, $HP = 0.5$, $Pr = 0.7$ and $D_P = 0.1$): (a) streamlines for $\varepsilon_e = 0.5$; (b) isotherms for $\varepsilon_e = 0.5$; (c) streamlines for $\varepsilon_e = 0.7$ and (d) isotherms for $\varepsilon_e = 0.7$.

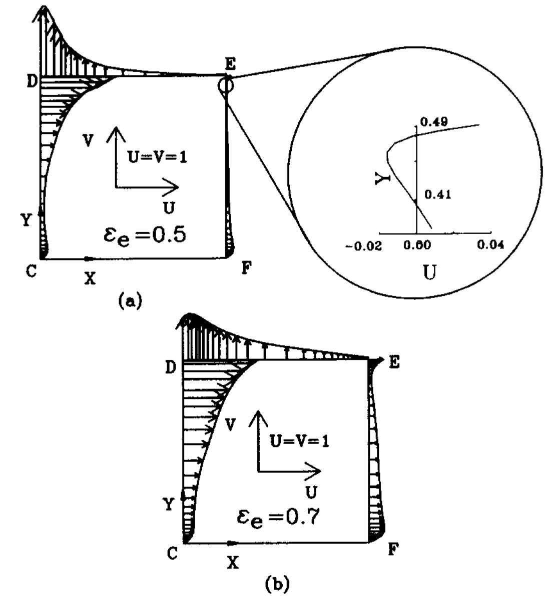

Fig. 5. Normal velocity distributions on the interfacial surface of the porous block ($Re = 500$, $HP = 0.5$, $Pr = 0.7$ and $D_P = 0.1$): (a) $\varepsilon_e = 0.5$ and (b) $\varepsilon_e = 0.7$.

Fig. 5 for $\varepsilon_e = 0.5$ and 0.7 cases and the unit velocity vectors are shown in Figs. 5(a) and (b), respectively. Due to the larger porosity on the interface, most of the fluid flows through the porous block via the upper left corner, then the maximum velocity appears on this corner. The velocity which flows from the porous block on the rear surface of the porous block increases as the porosity increase. Due to the effect of the downstream recirculation zone, as shown in Fig. 5(a), a small region with negative velocity exists near the upper right corner of the porous block, hence, the streamline of ψ (= 0.018) in Fig. 3 slightly turns into this corner.

The local Nusselt number Nu_s on the interfacial surfaces of the porous block is shown in Fig. 6 and defined as:

$$Nu_s = \frac{\left(\rho_f c_f \vec{v}_n (T - T_o) - k_e \dfrac{\partial T}{\partial \vec{n}}\right)_{\text{interface}}}{\dfrac{k_f (T_w - T_o)}{H}} \tag{30}$$

where $\vec{n}$ means normal and outward direction. The abscissa S in Fig. 6 is the dimensionless distance along the interfacial surface from C to F.

The trends of the Nu_s on the interfacial surfaces for both the $\varepsilon_e = 0.5$ and 0.7 cases are similar except on the top interfacial region ($0.5 \leqslant S \leqslant 1$). On the former

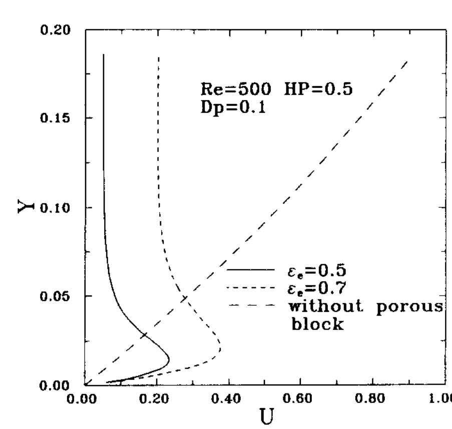

Fig. 4. U velocity profiles near the wall region at $X = 0.25$ (middle of the porous block) for $\varepsilon_e = 0.5$, 0.7 and 1.0 ($Re = 500$, $HP = 0.5$, $Pr = 0.7$ and $D_P = 0.1$).

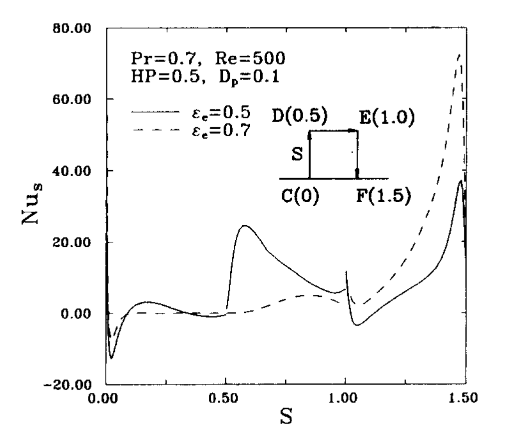

Fig. 6. Local Nusselt number Nu_S distributions on the interfacial surface of the porous block for $\varepsilon_e = 0.5$ and 0.7 ($Re = 500$, $HP = 0.5$, $Pr = 0.7$ and $D_P = 0.1$).

front interfacial surface ($0 \leqslant S \leqslant 0.1$) the Nu_s of both cases is negative which results from the isotherms extending upstream (shown in Fig. 3). In the region of ($0.1 \leqslant S \leqslant 0.5$), the values of Nu_s are approximately equal to zero which means heat transfer in this region is small. Consequently, the conduction heat transfer is dominant in the front interfacial surface. For $\varepsilon_e = 0.5$, the above phenomenon is more noticeable.

On the top interfacial surface ($0.5 \leqslant S \leqslant 1.0$), most of the fluid in the porous block are deflected toward the upper left corner of the porous block for the $\varepsilon_e = 0.5$ situation. Hence the Nu_s increases to the maximum value on this corner. However, for $\varepsilon_e = 0.7$ situation, most of the fluids flow through the porous block directly which causes the isotherms to extend downstream exclusively. As a result, the values of Nu_s are smaller than those of $\varepsilon_e = 0.5$ situation.

Due to the channeling effect, the Nu_s on the rear interfacial surface ($1.0 \leqslant S \leqslant 1.5$) has the maximum value close to the wall region for both cases. Large heat transfer occurs in this region. On the upper right corner, there is a small region with negative velocity as shown in Fig. 5(a), hence the values of Nu_s are negative for $\varepsilon_e = 0.5$ case.

The local Nusselt number Nu_x on the high temperature wall is defined as:

$$Nu_x = \frac{h_x H}{k_f} = -\frac{k_e}{k_f}\frac{\partial \theta}{\partial Y}\bigg|_{Y=0}. \tag{31}$$

As shown in Fig. 7, due to the large contact surface between the fluids and the porous block, the heat transfer is enhanced for both $\varepsilon_e = 0.5$ and 0.7 cases compared with the case without porous block. With higher velocity gradient on the wall for the $\varepsilon_e = 0.7$ case, the values of Nu_x for $\varepsilon_e = 0.7$ case are larger than those for the $\varepsilon_e = 0.5$ case. The results show little difference compared with Fig. 4 of Huang and Vafai [17]. The Nusselt number in [17] is defined in bulk temperature and both plates of the channel in [17] were high temperature region. For the lower Darcy number case (e.g. $\varepsilon_e = 0.5$ case), most of the flow was deflected away the porous block, as, in the previous discussion, which increased the heat transfer on the upper plate in [17], hence the Nusselt number in [17] increased due to the increase of the bulk temperature.

In Fig. 8, the streamlines and isotherms are illustrated for $Re = 500$, $HP = 0.5$, $\varepsilon_e = 0.5$, $Pr = 0.7$ and $D_P = 0.05$ and 0.2 cases. As the diameter of the spherical bead decreases, the drag force becomes larger under the same porosity condition. Consequently, for $D_P = 0.05$ situation, two recirculation zones in the upstream and downstream regions are formed, and the isotherms extend upstream as shown in Fig. 8. For $D_P = 0.2$ situation, only one recirculation zone is formed downstream, and the isotherms hardly extend upstream.

Based on the reason mentioned above, the larger the diameter is, the larger the velocity becomes. Hence the $D_P = 0.2$ case has the largest velocity distribution as indicated in Fig. 9. Because of the channeling effect, the maximum velocity exists near the wall. Accompanying the larger velocity gradient for the larger diameter situation, therefore, the local Nusselt number Nu_x distribution for $D_P = 0.2$ situation is larger than the other situations as illustrated in Fig. 10.

As the Reynolds number Re increases, the inertial force becomes stronger. As shown in Fig. 11, two recirculation zones are found in the upstream and

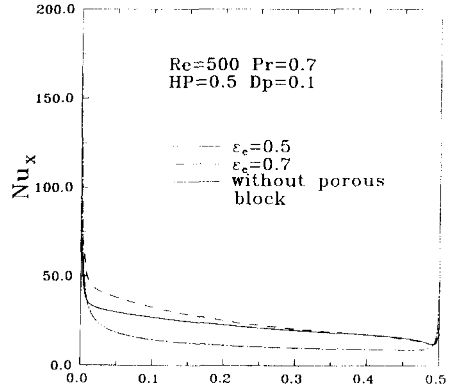

Fig. 7. Local Nusselt number Nu_x distributions on the high temperature wall for $\varepsilon_e = 0.5$, 0.7 and 1.0 ($Re = 500$, $HP = 0.5$, $Pr = 0.7$ and $D_P = 0.1$).

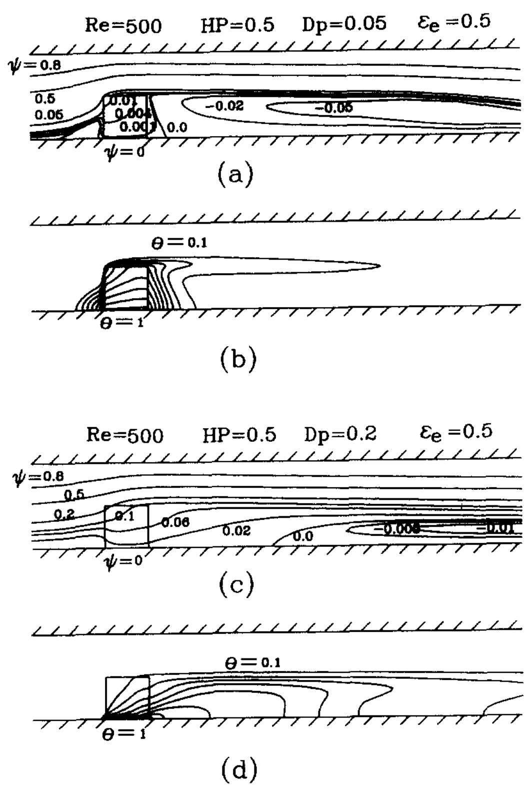

Fig. 8. Effect of particle diameter on flow field and thermal field ($Re = 500$, $HP = 0.5$, $Pr = 0.7$ and $\varepsilon_e = 0.5$): (a) streamlines for $D_P = 0.05$; (b) isotherms for $D_P = 0.05$; (c) streamlines for $D_P = 0.2$ and (d) isotherms for $D_P = 0.2$.

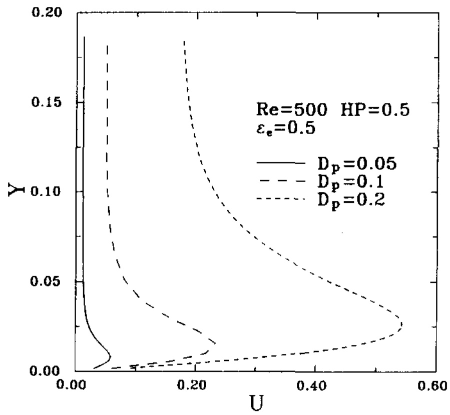

Fig. 9. U velocity profiles near the wall region at $X = 0.25$ (middle of the porous block) for $D_P = 0.05$, 0.1 and 0.2 ($Re = 500$, $HP = 0.5$, $Pr = 0.7$ and $\varepsilon_e = 0.5$).

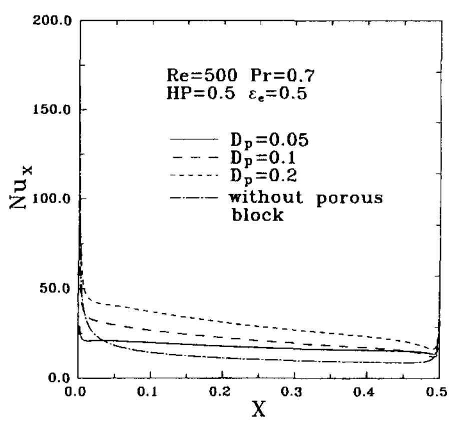

Fig. 10. Local Nusselt number Nu_x distributions on the high temperature wall for $D_P = 0.05$, 0.1 and 0.2 ($Re = 500$, $HP = 0.5$, $Pr = 0.7$ and $\varepsilon_e = 0.5$).

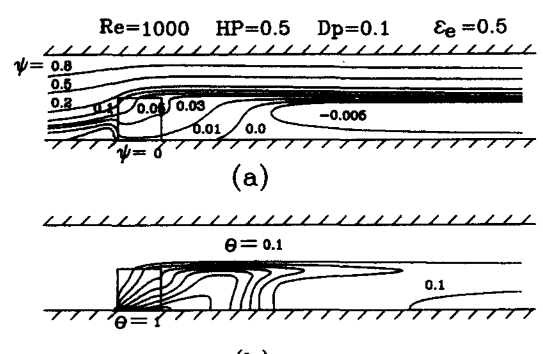

Fig. 11. Effect of Reynolds number Re on flow and thermal fields ($Re = 1000$, $HP = 0.5$, $D_P = 0.1$, $Pr = 0.7$ and $\varepsilon_e = 0.5$) : (a) streamlines and (b) isotherms.

downstream regions, respectively, and the isotherms extend downstream more significantly. Due to the stronger inertial force for the higher Reynolds number ($Re = 1000$) situation, not only more fluid flows through the porous block but also the fluid had higher velocity pass through the porous block which certainly causes the local Nusselt number Nu_x distribution to be larger than those of the lower Reynolds number ($Re = 500$) and the without-porous-block ($Re = 1000$) situation as shown in Fig. 12.

For $HP = 1.0$ cases, the streamlines and the isotherms are shown in Fig. 13 for $Re = 500$, $HP = 1.0$, $D_P = 0.1$ and $\varepsilon_e = 0.5$. The streamlines, compared with Fig. 3(a), show that there are no recirculation zones in both the front and rear sides of the porous media. Meanwhile the fluids are forced to flow through the near wall regions because of the channeling effect. Hence the isotherms concentrate more near the wall and expand to the downstream as shown in Fig. 13(b).

The U velocity profiles along the Y axis at the middle ($X = 0.25$) of the porous block for $Re = 500$ are shown in Fig. 14. The smaller the D_P and ε_e are, the larger the drag force becomes, which causes more fluids to flow near the wall. As a result, the case of $D_P = 0.05$ and $\varepsilon_e = 0.5$ has the largest velocity gradient near the wall. The phenomena are opposite to that of the $HP = 0.5$ cases as shown in Figs. 4 and 9.

The effects of the porosity on the Nu_x in the $HP = 1.0$ cases are illustrated in Fig. 15. Due to the behaviors of the channeling effect shown in Fig. 14,

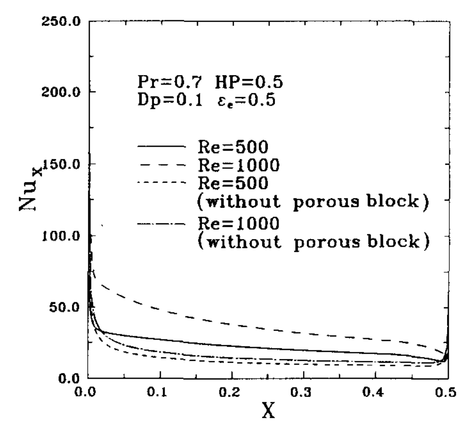

Fig. 12. Local Nusselt number Nu_x distributions on the high temperature wall for $Re = 500$ and 1000 ($D_P = 0.1$, $Pr = 0.7$ and $HP = 0.5$).

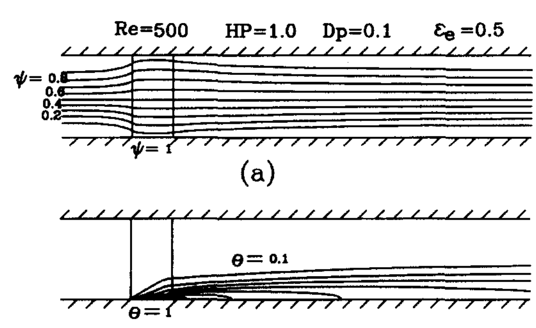

Fig. 13. Effect of blocked ratio HP on flow and thermal fields ($Re = 500$, $HP = 1.0$, $D_P = 0.1$, $Pr = 0.7$ and $\varepsilon_e = 0.5$) : (a) streamlines and (b) isotherms.

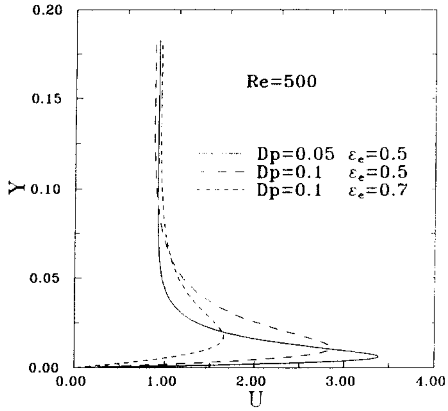

Fig. 14. U velocity profiles near the wall region at $X = 0.25$ (middle of the porous block) for $HP = 1.0$ case ($HP = 1.0$, $Pr = 0.7$ and $Re = 500$).

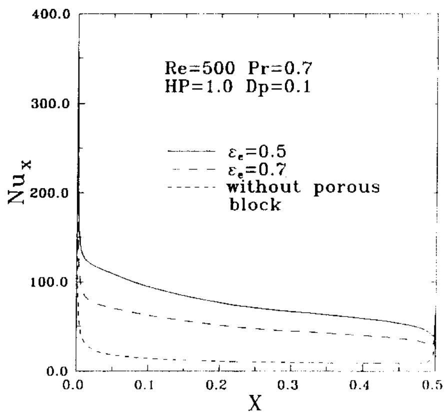

Fig. 15. Local Nusselt number Nu_x distributions on the high temperature wall for $HP = 1.0$ case with $\varepsilon_e = 0.5$ and 0.7 ($HP = 1.0$, $Re = 500$, $D_P = 0.1$ and $Pr = 0.7$).

the Nu_x of the $\varepsilon_e = 0.5$ case is higher than that of the $\varepsilon_e = 0.7$ case. This is opposite to the results of the $HP = 0.5$ cases shown in Fig. 7. Because of the effects of the particle diameter D_P, Fig. 16 shows that smaller particle diameter induces higher heat transfer in the

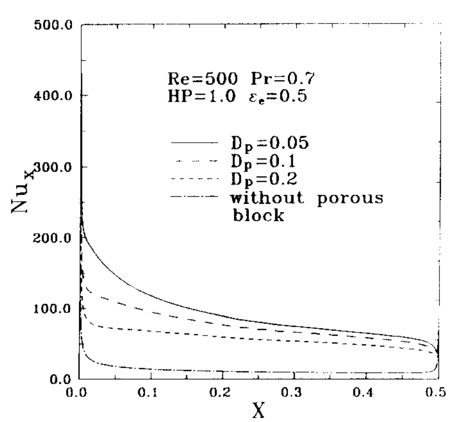

Fig. 16. Local Nusselt number Nu_x distributions on the high temperature wall for $HP = 1.0$ case with $D_P = 0.05$, 0.1 and 0.2 ($HP = 1.0$, $Re = 500$, $\varepsilon_e = 0.5$ and $Pr = 0.7$).

$HP = 1.0$ cases. These results are also opposite to the results of the $HP = 0.5$ cases.

CONCLUSIONS

In this paper, the thermal performance of a channel mounted with a porous block in laminar flow is studied numerically. The results can be summarized as follows:

(1) The thermal enhancement could be obtained by a copper porous block mounted on the high temperature region.

(2) A porous block with higher porosity in a $HP = 0.5$ channel could increase the heat transfer. However the result is opposite to that of the $HP = 1.0$ channel.

(3) In $HP = 0.5$ channel, the heat transfer could be enhanced by a porous block with higher particle diameter. This result is also opposite to that of the $HP = 1.0$ channel.

Acknowledgement—The support of this work by National Science Council, Taiwan, R.O.C. under contract NSC83-0401-E-009-454 is gratefully acknowledged.

REFERENCES

1. K. Vafai and C. L. Tien, Boundary and inertia effects on flow and heat transfer in porous media, *Int. J. Heat Mass Transfer* **24**, 195–203 (1981).
2. M. Kaviany, Laminar flow through a porous channel bounded by isothermal parallel plates, *Int. J. Heat Mass Transfer* **28**, 851–858 (1985).
3. R. F. Benenati and C. B. Brosilow, Void fraction distribution in a bed of spheres, *A.I.Ch.E. J.* **8**, 359–361 (1962).
4. K. Vafai, Convection flow and heat transfer in variable-porosity media, *J. Fluid Mech.* **147**, 233–259 (1984).
5. K. Vafai, R. L. Alkire and C. L. Tien, An experimental investigation of heat transfer in variable porosity media, *J. Heat Transfer* **107**, 642–647 (1985).
6. P. Cheng and C. T. Hsu, Fully-developed forced convective flow through an annular packed-sphere bed with wall effects, *Int. J. Heat Mass Transfer* **29**, 1843–1853 (1986).
7. P. Cheng and C. T. Hsu, Applications of Van Driest's mixing length theory to transverse thermal dispersion in a packed-bed with boundary walls, *Int. Commun. Heat Mass Transfer* **13**, 613–625 (1986).
8. P. Cheng and H. Zhu, Effects of radial thermal dispersion on fully-developed forced convection in cylindrical packed tubes, *Int. J. Heat Mass Transfer* **30**, 2372–2383 (1987).
9. P. Cheng, C. T. Hsu and A. Chowdhury, Forced convection in the entrance region of a packed channel with asymmetric heating, *J. Heat Transfer* **110**, 946–954 (1988).
10. C. T. Hsu and P. Cheng, Thermal dispersion in a porous medium, *Int. J. Heat Mass Transfer* **33**, 1587–1597 (1990).
11. G. S. Beavers and D. D. Joseph, Boundary condition at a naturally permeable wall, *J. Fluid Mech.* **30**, 197–207 (1967).
12. K. Vafai and R. Thiyagaraja, Analysis of flow and heat transfer at the interface region of a porous medium, *Int. J. Heat Mass Transfer* **30**, 1391–1405 (1987).
13. K. Vafai and S. J. Kim, Fluid mechanics of the interface region between a porous medium and a fluid layer—

an exact solution, *Int. J. Heat Fluid Flow* **11,** 254–256 (1990).
14. K. Vafai and S. J. Kim, Analysis of surface enhancement by a porous substrate, *J. Heat Transfer* **112,** 700–706 (1990).
15. P. C. Huang and K. Vafai, Flow and heat transfer control over an external surface using a porous block array arrangement, *Int. J. Heat Mass Transfer* **36,** 4019–4032 (1993).
16. A. Hadim, Forced convection in a porous channel with localized heat sources, *J. Heat Transfer* **116,** 465–472 (1994).
17. P. C. Huang and K. Vafai, Analysis of forced convection enhancement in a channel using porous blocks, *AIAA J. Thermophys. Heat Transfer* **8,** 563–573 (1994).
18. J. P. Van Doormaal and G. D. Raithby, Enhancements of the SIMPLE method for predicting incompressible fluid flows, *Numer. Heat Transfer* **7,** 147–163 (1984).
19. S. V. Pantankar, *Numerical Heat Transfer and Fluid Flows.* Hemisphere, Washington D.C. (1980).